Numerical Verification for Seismic Response of Reinforced Soil Embankment on Soft Clay Foundation

Ripon Hore[1 and 2], Sudipta Chakraborty[3], Kamruzzaman Kamrul[4], Ayaz Mahmud Shuvon[3], and Mehedi A. Ansary[4]
[1]*LGED, Dhaka, Bangladesh*
[2]*East West University, Dhaka, Bangladesh*
[3]*Bangladesh Network Office for Urban Safety (BNUS), Bangladesh University of Engineering and Technology, Dhaka, Bangladesh*
[4]*Department of Civil Engineering, Bangladesh University of Engineering and Technology, Dhaka, Bangladesh*
E-mail: riponhore@gmail.com

ABSTRACT: The findings of a series of shaking table tests and numerical analysis using PLAXIS 3D software to investigate the seismic influence of wrap-faced geotextile-reinforced embankment lying on soft clayey soil were presented in this paper. The test scheme included a succession of 1D Shake Table Tests (STT) with 0.05g to 0.2g base acceleration on a 0.4 m high model, lying on a 0.3 m thick, soft clay layer. This research aimed to understand the dynamic behavior of the model embankment resting on soft clayey soil. Both experimental and computational numerical studies were conducted to meet this purpose. The experimental study was a model study using a shake table. To assess the seismic behavior, harmonic sinusoidal input motions were subjected towards the model with different frequencies. The base acceleration, frequencies, and surcharge load were varied in several shake table tests with different relative densities of 48% for Sylhet sand. The pore water pressure and strain were also influenced by the base excitation, frequency, and surcharge pressure. The results obtained from PLAXIS 3D were compared with those obtained from model shake table tests. Acceleration response increased an increase of the base acceleration, the change further visible at higher elevations. The pore water pressures and strain values increased with elevation but decreased with the surcharge load. The strains were smallest at the bottom layer, and the strains at the top layer were the highest. The reason behind this is the geotextiles that are placed in the top layers. It enhances the earthquake strength of the embankment with a reinforced wall. The value of the findings from the test result was lower than the numerical result; the deviation was less than 15%. These results help to predict the dynamic behavior of the reinforced embankment wall. It will also help to design this type of retaining wall in the construction sector of Bangladesh.

KEYWORDS: Dynamic responses, soft clay foundation, Model reinforced wall, Variable input motions, PLAXIS 3D.

1. INTRODUCTION

Many attempts have been made in recent decades to explicate the dynamic characteristics of geosynthetic reinforced soil walls exposed to seismic motions through physical modeling using shake table tests (Ling et al., 2005; Latha and Krishna, 2006; El-Emam Bathurst, 2007; Damians et al., 2021; Srilatha et al., 2014; El-Emam, 2018; Hore et al., 2021). Richardson and Lee (1975) were the precursors of shaking table tests on scaled soil model walls. Srilatha et al. (2013) and Edinçliler and Toksoy (2017) conducted a study on shaking table tests in a compact scale on a model embankment. The purpose was to compare the results of a reinforced embankment under dynamic loading. Yazdandoust (2017) performed a series of shaking table tests on a 0.9 m high model wall applying harmonic seismic loadings. The purpose of this experiment was to analyze the outcomes to make scientific predictions on the characteristics of the models. Furthermore, Zhou et al. (2019) showed another shaking table test of the high embankment model, which tested three different types of aeolian sand. A few other researchers (Zhang et al., 2009; Chen et al., 2010; Moss et al., 2010; Cheng et al., 2018) conducted shaking table tests to study the seismic responses of the soil model wall lying on soft clay to assess the effects of pore pressure.

Moreover, several numerical simulations (Elgamal et al., 2002; Chen et al., 2008; Jafarzadeh et al., 2008; Li et al., 2016; Kanty et al., 2016; Wu et al., 2019; Zhou et al., 2019; Hore et al., 2021) were carried out based on the physical experiments to validate the experimental result. Anastasopoulos et al. (2010) performed a scale model shaking table test of a typical bar-mat retaining wall and compared the experimental results with the numerical outcomes by employing the finite element method using ABAQUS.

This paper analyzed the performance of a regular bar-mat retaining wall in both experimental and computation numerical methods. Bhattacharjee and Krishna (2013) analyzed the behavior of soil model walls through numerical analysis by using FLAC 3D. Moreover, Wulandaria et al. (2015) determined the optimum tensile strength of geotextile using PLAXIS 2D. They used the finite element method, considered the allowed factor of safety while considering the reinforcement in road embankment. Gidday and Mittal (2020) studied geotextile reinforced walls under dynamic conditions on a shake table; their findings showed that vertical apex settlement and lateral displacement of reinforced soil walls decrease when reinforcing layers increase. They used both cement-treated and clay soil without improvement as backfill soil, and numerical modeling was performed by PLAXIS 3D. The slope in the modeling was considered 45°, and sinusoidal shaking was used for 20 cycles. Chakraborty et al. (2021) studied the dynamic behavior of wrap-faced embankments on soft clay using an experimental (shake table) model. The various dynamic soil parameters such as pore water pressure and strain were analyzed.

This research analyzed the relative performance of seismic effect due to sinusoidal waves on geotextile-reinforced wrap-faced soil walls on soft clay in Bangladesh by carrying out shaking table tests. The results of the shaking table tests are then compared with results from numerical analysis modeled in PLAXIS 3D. The base motion parameters are changed in different model tests for both experimental and numerical analysis.

2. OBJECTIVES AND SCOPE

This study is conducted for the following purposes: (a) to determine the performance of the model soil wall under sinusoidal loading conditions, (b) to choose a suitable scaling factor for the development of the model, (c) to perform several shaking tests on a particular scale model embankment, (d) study the performance of the model by varying surcharge load, frequency, and acceleration (e) prepare similar model by PLAXIS 3D software, and (f) determine the dynamic parameters (Pore water pressure, and strain) by using both the shaking table test and computational numerical analysis (PLAXIS 3D).

3. SHAKING TABLE TESTING FACILITY

A shaking table facility used for our experiment is shown in Figure 1. The base is made of steel, and the platform has a length of 2 m and a

width of 2 m. The table has a payload capacity of 1500 Kg. Furthermore, it is maneuverer by a servo-hydraulic motor, with a single degree of freedom. The table can operate in a wide acceleration and frequency range, varying from 0.05g to 2g and 0.05 Hz to 50 Hz. Also, the maximum displacement along the axis of motion has a range of ±200 mm. The machine was operated at a velocity of 30 cm/sec.

Figure 1 Final setup of the shaking table tests

A laminar box is used as the container for this experiment, which was designed under a few considerations; maintaining a little cross-section, water tightness of the model, very low resistance to soil settlement, and having minimum shear stiffness and little mass. The box works as a large shear box with 24 hollow aluminum layers, as shown in Figure 1. The container is designed in a way that the saturated granular soil can deform freely when subjected to a seismic motion. The container has several components, the base plate and the saturation and drainage system in the floor, the upper and the side guides, layers, and ball bearings, and an elastic internal membrane. The upper and side guides prevent the frame from any kind of deformation and hold it strongly. The ball bearings diameter is 12 mm. The ball bearings are placed in a hemispherical space to reduce the friction working as a column between the lower and upper hollow aluminum sections, reducing the surface's deformation.

Each layer has an inner frame. The measurement of the laminar box is 915 mm × 1220 mm × 1220 mm. The distance between any two consecutive layers is 2 mm. Also, an embankment is constructed with soft clayey soil to reduce the boundary effect. The base layer is attached strongly with the base plate, which has an equal base dimension to the inner frame, only the height is 15 mm.

3.1 Scaling Laws for Prototype

Though the scale soil model was developed properly, achieving similarity with the prototype soil wall could not be ensured. In low-stress limits, shaking table tests can't predict the exact results of the prototype. But when it comes to the reinforced model wall, the prediction becomes relatively accurate (Sabermahani et al., 2009; Latha and Krishna, 2008; Krishna and Latha, 2007; Chakraborty et al., 2021). Also, the bond among soils, geotextiles, and tensile strength, when scaled, require similitude requirements to be fulfilled. Viswanathan and Mahajan previously mentioned this matter in 2007. Table 1 represents the assumed values of the factors. We assumed $\alpha = 0.5$ for sand, as per the earlier literature of Kokusho (1980) and Yu and Richart (1984).

3.2 Input Motions

Earlier literature by Sabermahani et al. (2009) showed that the sinusoidal base acceleration has more strength and can cause more damage than a typical seismic motion having the same amplitude and fundamental frequency. This theory was already reviewed in the literature published earlier by Bathurst and Hatami (1998), Matsuo et al. (1998), and El-Emam and Bathurst (2007). In this study, the fundamental frequency was around 10 Hz for the model wall. To avoid resonance, the applied frequency should be lower than the fundamental frequency of the wall. Typically, frequencies ranging between 2 Hz and 3 Hz represent frequencies observed in typical earthquakes (Bathurst and Hatami, 1998; Chakraborty et al., 2021).

Table 1 Item wise scale factor

No.	Items	Scale factor (empirical)	Scale factor (Prototype/Model)
1	Acceleration (a)	1	1
2	Density (ρ)	1	1
3	Length (L)	1/N	10
4	Stress (σ)	1/N	10
5	Strain (ε)	$1/N^{1-\alpha}$	3.125
6	Stiffness (G)	$1/N^{\alpha}$	3.125
7	Displacement (d)	$1/N^{2-\alpha}$	32.25
8	Frequency (f)	$N^{1-\alpha/2}$	0.18
9	Force (F)	$1/N^{3}$	1000
10	Shear Wave Velocity (V_s)	$1/N^{\alpha/2}$	1.785
11	Time (t)	$1/^{N1-\alpha/2}$	5.62

Some studies were conducted with low amplitude base accelerations, i.e., 0.1g to 0.2g (Krishna and Latha 2007; Latha and Manju 2016; Helwany et al. 2017; Hore et al., 2021). Also, some studies were conducted with higher amplitude, varying from 0.3g to 0.5g (Sabermahani et al. 2009; Edinçliler and Toksoy 2017; Damians et al. 2021). For peak base acceleration, both low and high amplitude values were taken, with 0.05g being the low and 0.2g being the high value. In total, harmonic sinusoidal shaking was applied nine times, as shown in Table 2.

Table 2 Test Parameters for Model

Test Name	Surcharge Load*, kPa	Base Acceleration, g	Frequency, Hz	Relative Density, %
ST1	1.72	0.05	1	48
ST2	1.72	0.05	2	48
ST3	1.72	0.05	3	48
ST4	1.72	0.05	5	48
ST9	1.72	0.1	1	48
ST19	1.72	0.15	1	48
ST27	1.72	0.2	1	48
ST35	1.12	0.05	1	48
ST67	0.70	0.05	1	48

*A Scale factor of 10 was used for Phototype

4. MODEL SOIL PROPERTIES AND PREPARATION

The total model consisted of a 300 mm soft clayey soil foundation, followed by 50 mm of sand blanket separated through a geotextile and 400 mm of wrap-faced sandy soil wall. One of the most significant factors that dominate scale effects and also the response of the model is the Model wall height, concerning the prototype height. The diagram of wrap faced embankment model wall is shown in Figure 2.

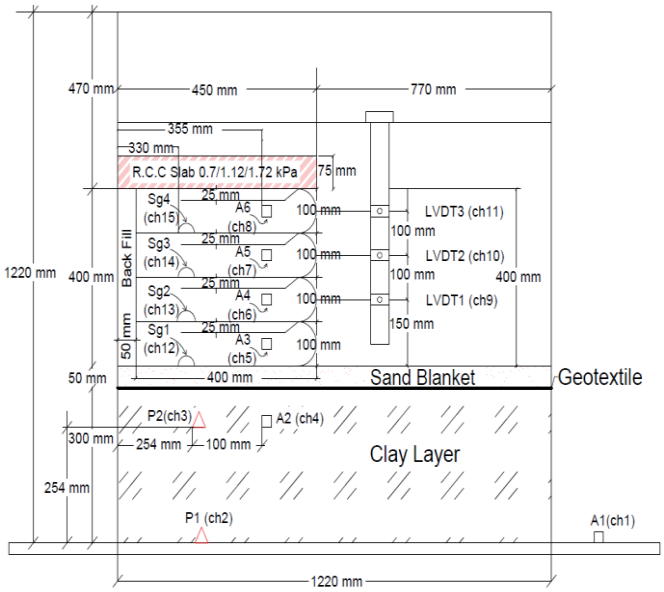

Figure 2 Diagram of wrap faced embankment model wall

4.1 Soft Clayey Soil

From the soil test, its fundamental soil properties are determined. The unit weight of the soil is found to be 14.8 KN/m3. The specific gravity of the clayey soil is 2.72. The undrained shear test showed that its shear strength is 28 kPa. The bearing capacity of the soil is 17.2 kPa. The average Liquid Limit and Plastic Limit (PL) value is 41% and 16%, respectively. The Plastic Limit for the soil is located below the A-line, calculated from the relation PI = 0.73(LL-20). As per the Unified Soil Classification System (USCS), the soil is found to be Lean Clay (CL). Then the soil was reconstructed by A 'Hobart' rotary mixer according to Burland (1990) as described in Hore et al. (2021). The thickness of the reconstituted Clay layer [the initial water content is equal to the Liquid Limit (LL)] of the sample was 300 mm in the laminar shear box. Then one-dimensional consolidations were taken place. The drained condition at loads (15 kPa, 20 kPa, 25 kPa, 30 kPa, 40 kPa, 60 kPa, 80 kPa, and 100 kPa) were placed. A 'Hobart' rotary mixer was used, as presented in Figure 3. The placement of clay soil and conduction of the unconsolidated undrained (UU) test is illustrated in Figure 4. The isotropic condition at loads with sensor arrangement is shown in Figure 5. The average settlement curve is depicted in Figure 6.

Figure 3 (a) The soft clay soil before oven-dry, (b) Soil after oven-dry (c) Dry sample in a bag, and (d) The mixing of sample to gain liquid limit

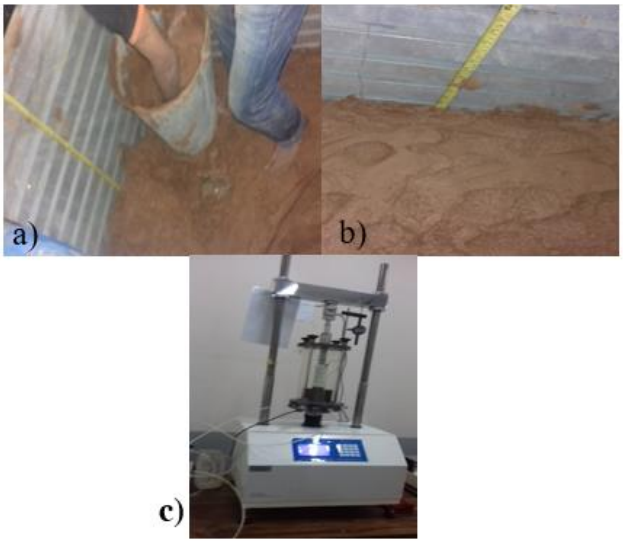

Figure 4 (a) The clay soil on Laminar box b) Showing clay soil on Laminar box, and c) The process of lab test (UU)

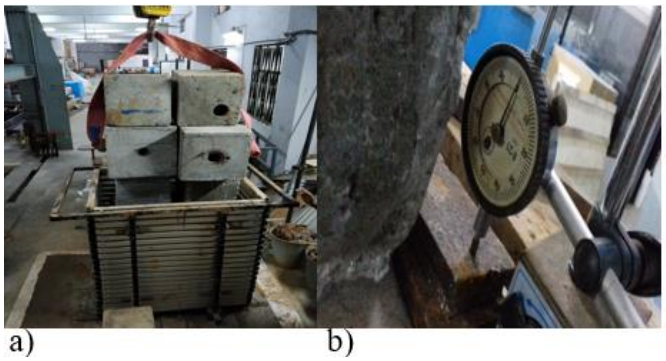

Figure 5 (a) The Loading system for Reconstituted Clay Layer Preparation, and 5 (b) Showing the displacement record

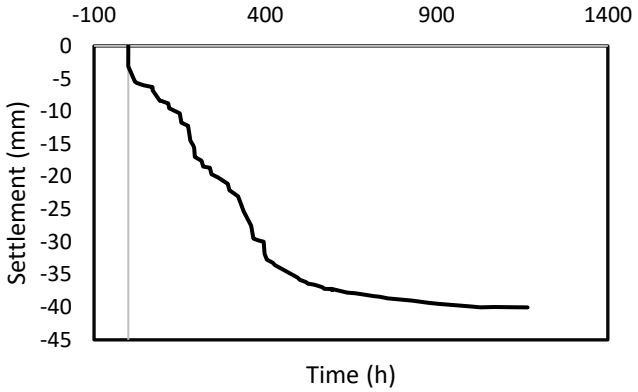

Figure 6 Average time settlement curve

4.2 Sandy Soil and Reinforcement

The sand was used to develop the 0.4 m (16") enhanced reinforced soil zone and backfill soil. To analyse its characteristics, the sample was dried in an oven, then sieved through standard sieves standardized by ASTM. The passing Sieve was #4, and the retaining sieve was #200. The distribution of the size of the particles is illustrated in Figure 7. From Figure 7, the Coefficient of uniformity (Cu) and coefficient of curvature (Cz) values were found to be 3.08 and 0.88, respectively, which dictates that the sample is poorly graded, medium to fine sand (SP). Also, the FM value of the Sylhet sand was found to be 2.031. The value of Specific Gravity (Gs), maximum dry density, and minimum dry density was found 2.65, 16.6 kN/m3, 13.8 KN/m3. To govern the sand density and sustain the different heights to acquire respective relative densities, a portable pluviator,

developed by Hossain and Ansary (2018), was used, demonstrated in Figure 8. The value of relative density of the Sylhet sand was 48%, and the test result inferred that the angle of internal friction's (ϕ) value is 34 (degree).

To reinforce the sand in the test, A woven polypropylene multifilament geotextile (D50) is used. This individual multifilament is developed in such a way that it ensures the stability of each of the dimensions. The relevant properties and the characteristics are of the multifilament are shown in Table 3. Geotextile with an area of 1 m^2 was placed between these two layers of clayey soil and sand blanket. The entire dimension of the geotextiles wrap-around was 1.10 meters.

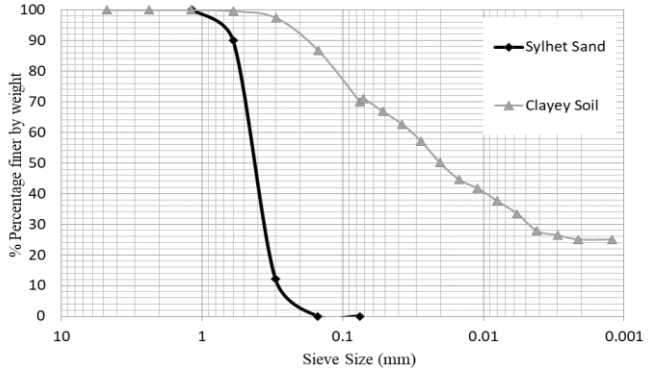

Figure 7 The distribution curve of particle size

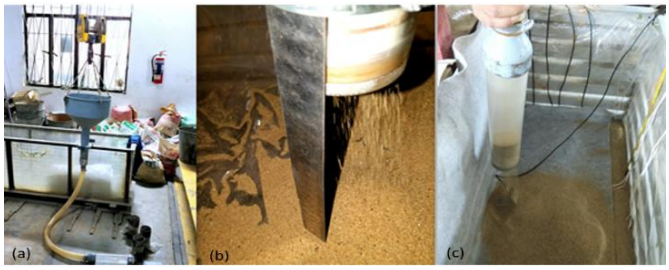

Figure 8 (a) Portable pluviator has been fitted with a crane for the development of model wall, (b) a scale has been attached with the diffuser for maintaining an accurate height of fall, and (c) the construction of layer of the model wall with pluviator

Table 3 Geotextile specification

No.	Details	Properties of geotextile
1	Reinforcement type	mechanically bonded needle punched
2	Yarn material (staple Fibre)	Polypropylene
3	Mass/unit area (gsm)	322
4	Aperture Size, O95 (μm)	130
5	Thickness (mm)	2.54
6	Ultimate Tensile Strength (KN/m)	15.5
	Ultimate Tensile Strength at 2% strain (KN/m)	15.97
	Ultimate Tensile Strength at 5% strain (KN/m)	16.57

4.3 Experimental Model with Different Sensor Arrangement

Four different types of sensors were deployed in the model to measure the acceleration, displacement, shear strain, and pore water pressure. For monitoring and measuring the accelerations of the developed model along with a vertical array, Accelerometers were used. To monitor the movement of the sand model wall along the horizontal direction, LVDT transducers were deployed. Four strain gauges were attached to the geotextile to measure the shear strain response. And finally, two sensors that measure pore-water pressure are positioned. In total, fifteen data channels are used; the arrangements are shown in Figure 2. To conclude, six accelerometers (A1, A2, A3, A4, A5, and A6), two-pore water pressure sensors (P1 and P2), four strain gauges (Sg1, Sg2, Sg3, and Sg4), and three linear variable differential transformers (LVDT1, LVDT2, and LVDT3) were positioned. The detailed layout of the experimental model is shown in Figure 2. Figure 9 shows the pore water pressure sensor. Figure 10 (a) and (b) show the strain and acceleration sensor. Figure 11 (a) shows finalized wrap-faced wall, 11 (b) shows three allocated LVDTs, 11 (c) presents the surcharge load, and 11 (d) shows the connecting board of all the strain gauges. Among the accelerometer sensors, the first sensor (A1) records the base acceleration. A2, A3, A4, A5, and A6 accelerometers were placed at 457 mm, 710 mm, 810 mm, 915 mm, and 1015 mm elevations, respectively, where the elevations are measured from the base. A3, A4, A5, and A6 were positioned uniformly, and the distance was 100 mm between any two consecutive sensors. Two pore water pressure sensors (P1 and P2) are used. The first one (P1) was placed at the bottom of the Clayey soil layer and the second one (P2) was placed at 457 mm. The pore water sensor arrangement is illustrated in Figure 9. Among the strain gauges, Sg1 was positioned above the sand blanket, at the base of the first layer. The remaining three strain gauges (Sg2, Sg3, and Sg4) were positioned at 100 mm, 200 mm, 300 mm elevation, respectively, maintaining a fixed 100 mm distance from the bottom facing of each layer. The wire attached with strain gauges was finally connected to the board directly linked to the digital data logger. Three displacement transducer sensors (LVDT1, LVDT2, and LVDT3) were positioned at 150 mm, 250 mm, and 350 mm elevations.

Figure 9 The pore pressure sensor (P2) at the desired location

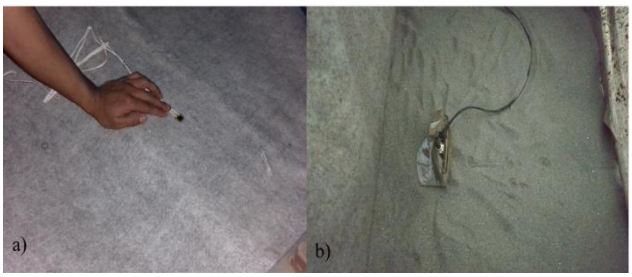

Figure 10 (a) The positioning of the strain gauge sensor (sg1) at the desired location and (b) The positioning of the Accelerometer sensor (A3) at the desired location

4.4 Surcharge Load and Relative Density

Three unlike surcharge loads with a value of 0.7, 1.12, and 1.72 kPa were used in this experiment. Three different types of concrete slabs, with a dimension of 24" × 18" × 3" (61 cm × 46 cm × 7.5 cm), 24" × 18" × 2" (61 cm × 46 cm × 5 cm), and 24" × 18" × 1" (61 cm × 46 cm × 2.5 cm), and weighed 49, 34 and 19.9 kg, respectively were used on this experiment. Chakraborty et al. (2021) described the procedure of surcharge load placement on the wrap-

faced model. After the construction of all the layers and placement of all sensors, a sinusoidal wave with an acceleration of 0.05g, 0.1g, 0.15g, and 0.2g was subjected to the model for every surcharge load variation.

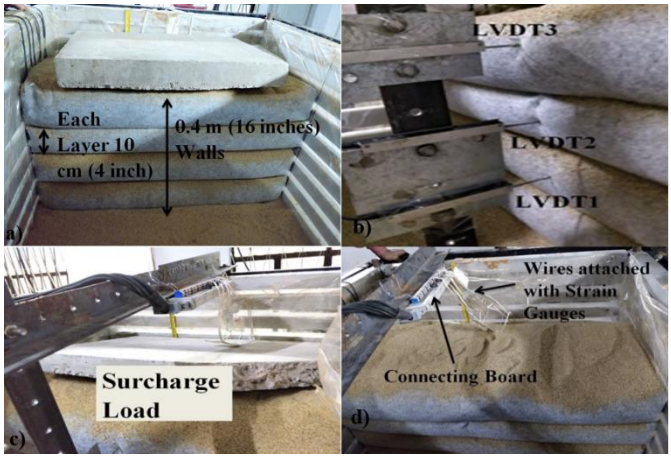

Figure 11 (a) The finalized wrap-faced wall (b) Three allocated LVDTs (c) The placement of surcharge load, and (d) The connecting board of all the strain gauges

5. DEVELOPMENT OF THE 3D NUMERICAL MODEL

The 0.4 m of wrap-faced embankments were used for the numerical modeling in this study. The PLAXIS 3D software (Brinkgreve and Broere, 2006), which uses quadratic tetrahedral 10-node elements, has been used for performing the current analyses. The simple graphical input procedures enable a quick generation of complex finite element models, and the enhanced output facilities provide a detailed presentation of computational results. A reduced 1/10 scaled model was used for the shake table experiment, depicted in Figure 2. Three types of surcharges, such as 0.7 kPa, 1.12 KPa, and 1.72 kPa, respectively, were considered for modeling the traffic load. The tensile strength is found to be 2500 KN/m for the geotextile reinforcement. In the research, two layers were used: soft clay layer and sandy soil layer or embankment layer. The hardening soil model was used in sandy soil layer and soft soil model used for the soft clay layer.

5.1 Geometry and Boundary Conditions

The embankment was 0.9 m wide. The wrap-faced embankment was vertical. As the model was symmetric, only half (for our experiment, right half) was modeled and a section with a width of 0.2 m was considered in this study. At the uppermost surface of the soft Clay soil, sandy soil was used for the wrap-faced embankment. The subsoil comprises 0.3 m of soft soil. The 0.3 m of this soft soil layer was modeled as Clay. The water level was located 0.35 m below the original ground surface. A title as a wrap-faced embankment model was set from the Quick Select dialog box. Model dimension was set as follows $x_{min} = 0$, $x_{max} = 2.6$, $y_{min} = 0$, and $y_{max} = 0.2$. The limitations and the boundary conditions of the model are shown in Table 4.

Table 4 Model Boundary condition

Location	Boundary Limits	$X_{min.}$	$X_{max.}$	$Y_{min.}$	$Y_{max.}$	$Z_{min.}$	$Z_{max.}$
Clay layer	X = 0 to 2.6 m Y = 0 to 0.2 m Z = -0.35 to -0.05 m	Free	Free	Fixed	Fixed	Fixed	Free
Sand layer	X = 0 to 2.6 m Y = 0 to 0.2 m Z = -0.05 m to 0	Free	Free	Fixed	Fixed	Free	Free
Bottom (Wrap faced)	X = 0 to 0.45 m Y = 0 to 0.2 m Z = 0 to 0.1 m	Free	Free	Fixed	Fixed	Free	Free
Middle 1 (Wrap faced)	X = 0 to 0.45 m Y = 0 to 0.2 m Z = 0.1 to 0.2 m	Free	Free	Fixed	Fixed	Free	Free
Middle 2 (Wrap faced)	X = 0 to 0.45 m Y = 0 to 0.2 m Z = 0.2 to 0.3 m	Free	Free	Fixed	Fixed	Free	Free
Top (Wrap faced)	X = 0 to 0.45 m Y = 0 to 0.2 m Z = 0.3 to 0.4 m	Free	Free	Fixed	Fixed	Free	Free

Table 5 Material properties of clay foundation and wrap faced embankment

Name of the Parameters	Symbol	Sandy soil	Clayey Soil	Unit
General				
Material model	Model	Hardening soil	Soft soil	-
Drainage type	Type	Drained	Under. (A)	-
Soil unit weight above the phreatic level	γ_{unsat}	15.0	15	kN/m^3
Initial void ratio	e_o	0.63	0.71	-
Parameters				
Secant stiffness in standard drained	E_{50}^{ref}	25.0* 103	-	kN/m^2
Tangent stiffness for primary oedometer loading	E_{oed}^{ref}	25.0* 103	-	kN/m^2
Unloading / reloading stiffness	E_{ur}^{ref}	75.0* 103	-	kN/m^2
Power for the stress-level dependency of stiffness	m	0.5	-	-
Modified compression index	λ	-	0.16	-
Modified swelling index	K	-	0.03	-
Cohesion	C	2.0	28.0	kN/m^2

Table 5 (cont.)

Name of the Parameters	Symbol	Sandy soil	Clayey Soil	Unit
Friction angle	Φ	30	1.0	°
Dilatancy angle	Ψ	4.0	0.0	°
Advanced: Set to	-	Yes	Yes	-
Groundwater				
Data set	-	USDA	USDA	-
Model	-	Van Genuchten	Van Genuchten	-
Soil type	-	Sand	Clay	-
< 0.002 mm	-	0.0	49.0	%
0.002 - 0.05 mm	-	0.0	18.0	%
0.05 - 2 mm	-	100.0	33.0	%
Set to default	-	Yes	Yes	-
Horizontal permeability (x-direction)	k_x	25.92	0.07	m/day
Horizontal permeability (y-direction)	k_y	25.92	0.07	m/day
Vertical permeability	K_z	25.92	0.07	m/day
Change of permeability	C_k	1- 1015	0.2	-
Interfaces				
Interface strength	-	Rigid	Rigid	-
Strength reduction factor	R_{inter}	1.0	1.0	-
Initial				
K_o determination	-	Automatic	Automatic	-
Over-consolidation ratio	OCR	1.0	1.0	-
Pre-overburden	POP	0.0	0.0	kN/m^2

5.2 Definition of Soil Stratigraphy

A borehole was developed at (0, 0, 0) and used to define the soil layers by using the structure's mode. Table 5 shows the material characteristics for both sandy and clayey soil which was used for the embankment. The level of water was situated at z = -0.35 m. The column specifies a value of -0.35 to Head in the borehole.

5.3 Definition of Structural Elements

In this section, the structure element was defined. The geotextile layer was modeled and defined their properties. To model geotextile, initially, a poly curve was drawn. To draw a poly curve, four-segment were created separately. The type of the segment and its characteristics are shown in Table 6. After creating the polyline, the polyline was selected for extrusion assign value of 0.2. Then the extrude object button was clicked. The creation of the geotextile layer is shown in Figure 12.

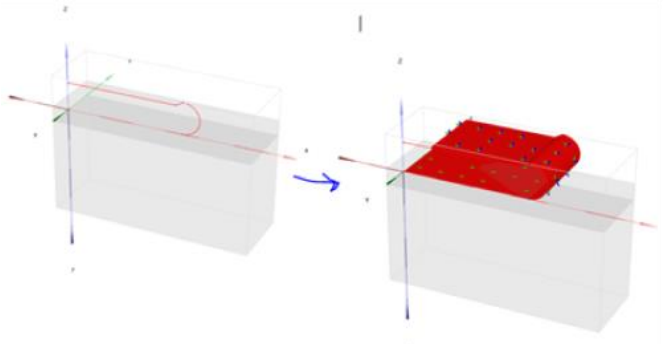

Figure 12 Created geotextile layer

5.4 Definition of Dynamic Multipliers and Mesh Generation

Dynamic loads were introduced based on the values of loads or given displacement used as input data, also the respective multipliers which are time-dependent. The load multipliers tab was selected for providing different dynamic parameters such as amplitude, phase, and frequency. For the mesh cohort, advance to the Mesh mode. Total volumes of the structure were selected, including the embankment. The Coarseness factor was 0.3. The whole wrap faced is shown in Figure 13.

Table 6 Structure construction by poly curve

Segment	Segment-1	Segment-2	Segment-3	Segment-4
Segment Type	Line	Arc	Line	Line
Properties of segment	Relative start angle = 0° Length = 0.35 m	Relative start angle = 0° Radius = 0.05 m Segment angle = 180°	Relative start angle = 30° Length = 0.025 m	Relative start angle = 30° Length = 0.35 m

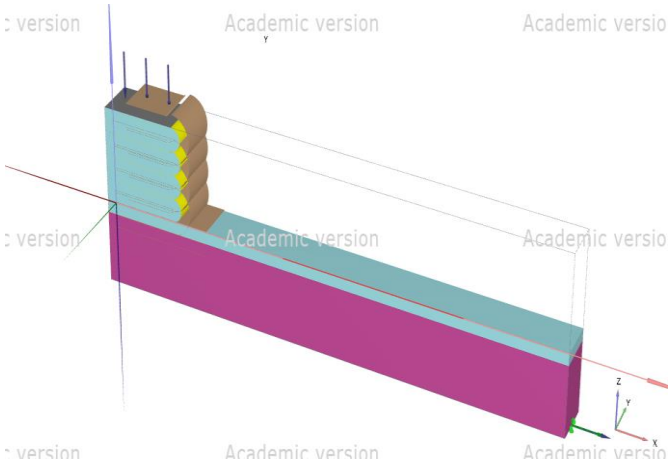

Figure 13 The whole wrap faced diagram

6. RESULTS AND DISCUSSION

Findings from twelve different shaking table tests on a scaled model embankment were conferred for experimental and numerical in this paper. In this research, only the surcharge load was varied with the fixed frequency of 1 Hz. The results are shown in Table 5 for different models varying different parameters. Sinusoidal wave motions were used as input dynamic motion. Four acceleration amplitudes (0.05g, 0.1g, 0.15g, and 0.2g) with a different frequency and surcharge were used for this experiment. The surcharge pressure on the embankment was kept as 0.5, 1.0, and 1.5 kPa. Every individual shaking table test was performed on the newly constructed model wall with maintaining the same relative density (48%) each time.

6.1 Pore Water Pressure Response of the Experimental and Numerical Model

The time records of the tests are depicted in Figure 14. For all elevations, the soil profile ST1-ST4, ST9, ST19, ST27, ST35, ST67, ST99, and ST193 were taken with 1.72 kPa, 1.12 kPa, and 0.7 kPa surcharge, 0.05g, 0.1g, 0.15g, and 0.2g base acceleration and 1 Hz-5 Hz frequency of sinusoidal motion subjected. The variations in pore water pressure are depicted in Figures 15-17. A 300 mm Clayey soil layer (S) was engaged for pore water pressure.

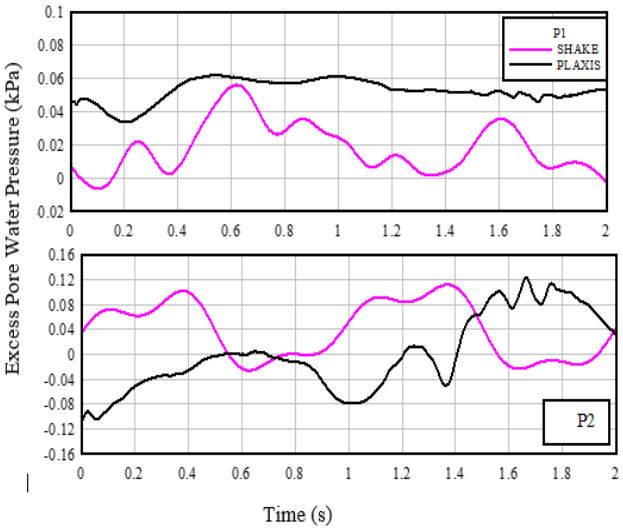

Figure 14 Excess Porewater Pressure response (Model ST1-Frequency 1 Hz, Acceleration- 0.05g, Relative density 48% and surcharge 1.72 kPa)

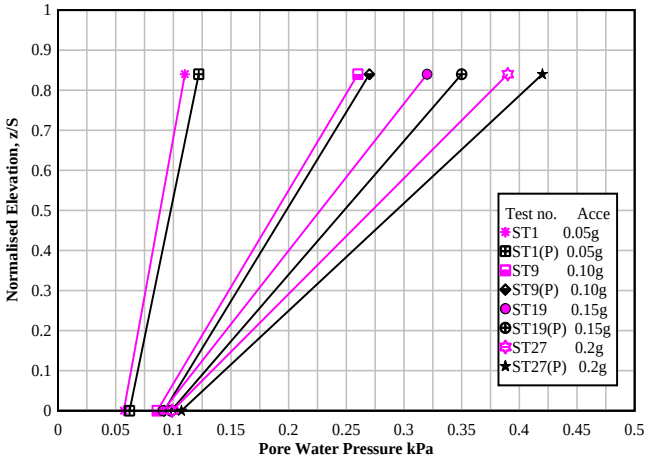

Figure 15 Effect of base acceleration on pore water pressure (ST1, 9, 19, and 27)

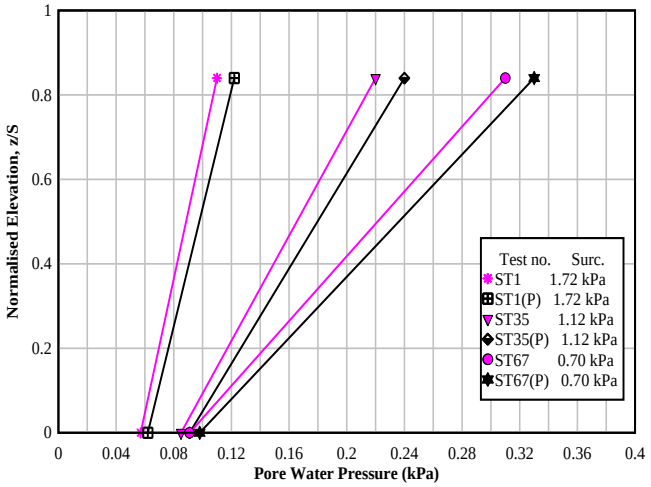

Figure 16 Effect of surcharge on pore water pressure (ST1, 35, and 67)

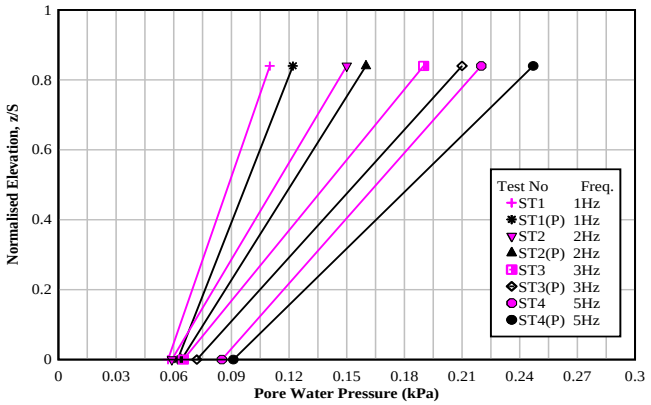

Figure 17 Effect of frequency on pore water pressure (ST1-ST4)

6.1.1 Effect of Input Acceleration

The change occurred in the value of the pore water pressure [model tests ST1, ST9, ST19, and ST27] with base accelerations 0.05g, 0.10g, 0.15g, and 0.20g, respectively for 1 Hz frequency and surcharge load of 1.72 kPa is shown in Figure 15. At z/S = 0.84, the pore water pressure response is directly proportional to base acceleration. The highest pore water pressure was 0.390 kPa at a base acceleration of 0.2g. The maximum pore water pressure for model tests ST1, ST9, ST19, and ST27 was 0.110 kPa, 0.260 kPa, 0.320 kPa, and 0.390 kPa, respectively. The figure also shows that the pore water pressure was 0.390 kPa at an acceleration of 0.2g, but dropped to 0.110 kPa at an acceleration of 0.05g is presented in Table 7. Pore water pressure escalated with base accelerations. Increasing the base accelerations creates shaking of the soil embankment and amplification was also increased (Higher lateral movement). Findings from PLAXIS 3D showed that pore water pressure [Profile for tests ST1(P), ST9(P), ST19(P), and ST27(P)] also at all elevations pore water pressure was directly proportional according to Figure 15. The figure also shows that the maximum pore water pressure was 0.420 kPa at an acceleration of 0.20 g, but was reduced to 0.122 kPa against an acceleration of 0.05 g. The values of highest and lowest pore water pressure obtained from PLAXIS 3D were 7.69% and 10.91% higher than the values obtained from shake table model tests. Figure 18 depicts the PLAXIS 3D output results of the porewater pressure response.

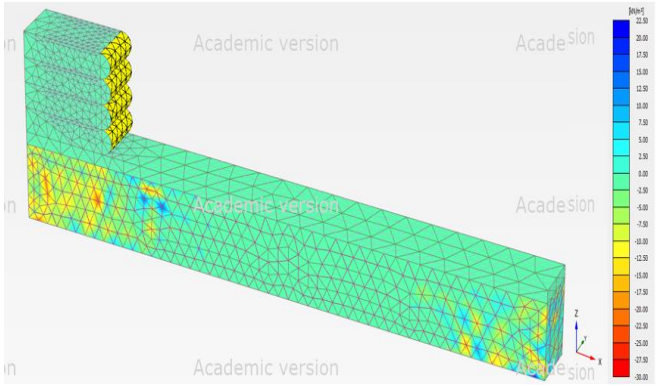

Figure 18 Pore water pressure response (ST2)

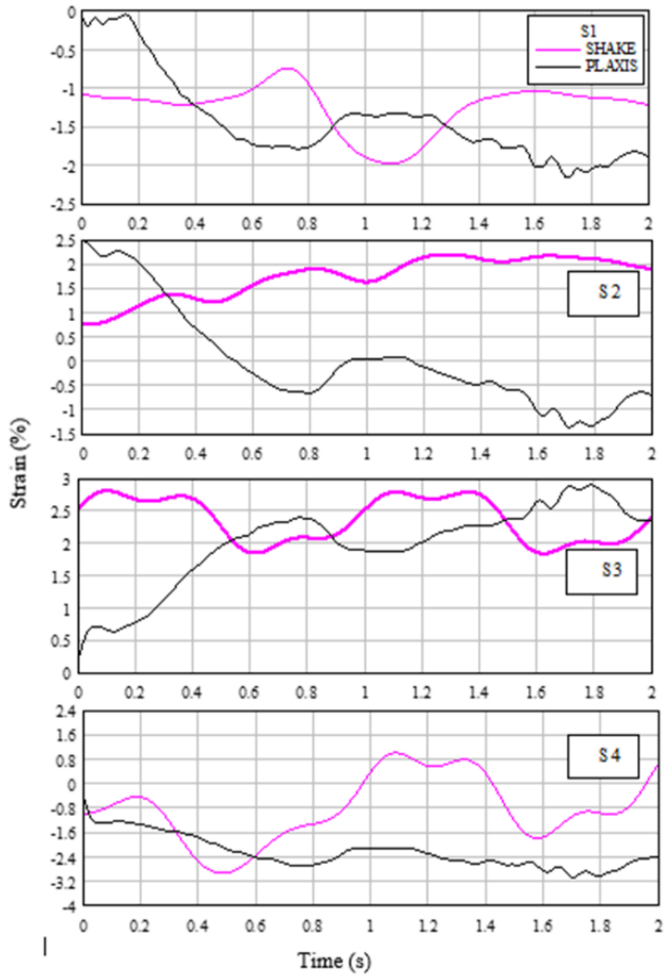

Figure 19 Strain Response (Model ST1-Frequency 1 Hz, Acceleration- 0.05g, Relative density 48% and surcharge 1.72 kPa)

6.1.2 Effect of Surcharge

For 1 Hz frequency and base acceleration of 0.20g, changes in the values of pore pressure [model tests ST1, ST35, and ST67] with surcharge load of 1.72 kPa, 1.12 kPa, and 0.7 kPa, respectively are depicted in Figure 16. The figure shows that the response of the pore water pressure with surcharge variation was inversely proportional at all elevations. The highest pore water pressure was 0.310 kPa at a surcharge load of 0.7 kPa. The highest pore water pressure [tests ST1, ST35, and ST67] were 0.110 kPa, 0.220 kPa, and 0.310 kPa, respectively. The figure also represents that the maximum pore water pressure was 0.310 kPa at a surcharge of 0.7 kPa, which later was reduced to 0.110 kPa at a surcharge of 1.72 kPa is presented in Table 7. At the top of the wall, the pore water pressure was inversely proportional to the surcharge pressure. When the surcharge pressure increases, the pore water dissipates. Therefore, the pore pressure decreased due to a large surcharge. Results obtained from PLAXIS 3D analysis showed that at all elevations, pore water pressure [Profile for tests ST1(P), ST35(P), and ST67(P)] pore water pressure varies inversely proportionally, as shown in Figure 16. Also, the maximum pore water pressure was 0.330 kPa at a surcharge of 0.7 kPa, which later dropped to 0.122 kPa at a surcharge of 1.72 kPa. The values of the highest and lowest pore water pressure obtained from PLAXIS 3D were found to be 6.45% and 10.91% higher than the results obtained from shake table tests.

Table 7 Response of Pore water pressure (Experimental and numerical)

Test Item	Dynamic Parameters	Location of sand layer	Experimental Results (kPa)	Numerical results (kPa)	Variation of Results (%)
ST1	Acceleration	P2 Location	0.110	0.122	10.91
ST9		P2 Location	0.260	0.270	3.85
ST19		P2 Location	0.320	0.350	9.37
ST27		P2 Location	0.390	0.420	7.69
ST1	Surcharge	P2 Location	0.110	0.122	10.91
ST35		P2 Location	0.220	0.240	9.09
ST67		P2 Location	0.310	0.330	6.45
ST1	Frequency	P2 Location	0.110	0.122	10.91
ST2		P2 Location	0.150	0.160	6.67
ST3		P2 Location	0.190	0.210	10.53
ST4		P2 Location	0.220	0.247	12.27

6.1.3 Effect of Input Frequency

For a provided base acceleration and surcharge load on pore water pressure (Tests ST1, ST2, ST3, and ST4), while varying the frequency by 1 Hz, 2 Hz, 3 Hz, and 5 Hz for 0.1g base accelerations and 1.72 kPa surcharge are shown in Figure 17. The figure infers that pore water pressure response against frequency variation was directly proportional. The highest pore water pressure was 0.220 kPa at 5 Hz frequency. The figure also shows that the highest pore water pressure was 0.220 at a frequency of 5 Hz, but dropped to 0.110 kPa at a frequency of 1 Hz (9). Finding obtained from PLAXIS 3D indicated that at all elevations, pore water pressure [Profile for tests ST1(P), ST2(P), ST3(P), and ST4(P)] was not directly proportional with frequency, as depicted in Figure 17. Figure 17 also infers that the highest pore water pressure was 0.247 kPa at a frequency of 5 Hz, but dropped to 0.122 kPa at a frequency of 1 Hz. The highest and lowest pore water pressure from PLAXIS 3D was 12.27% and 10.91% more than the shake table test, respectively.

6.2 Strain Response of the Experimental and Numerical Model

The strain time records of the shake table test ST1-ST4, ST9, ST19, ST27, ST35, ST67, ST99, and ST193 with 1.72 kPa, 1.12 kPa, and 0.7 kPa surcharge, 0.05g, 0.1g, 0.15g, and 0.2g base acceleration and 1 Hz - 5 Hz frequency of base sinusoidal motion at same elevation are shown throughout Figures 19. The Strain profiles from different tests after 20 cycles of sinusoidal motion are presented throughout Figures 20 to 22.

6.2.1 Effect of Input Acceleration

Figure 20 depicts the strain (%) profile for different base accelerations of 0.05g, 0.10g, 0.15g, and 0.20g from tests ST1, ST9, ST19, and ST27 respectively. The figure also indicates that the strain (%) was relatively high at higher base accelerations at the standardized elevation of z/H = 0.75. From the Figure, a maximum strain (%) of 3.45 of the total wall heights (H), for 0.20g, was recorded compared with 2.85 for 0.05g base accelerations. The figure also shows that the maximum strain (%) was 3.45 at an acceleration of 0.2g, whereas it decreased to 2.85 at an acceleration of 0.05g (Table 8). The strain was more at the peak height. Also, the overburden pressure was lower compared to the bottom of the wall. For this reason, at the bottom of the wall, percentage deformation was less due to higher overburden pressure [surcharge and wrap faced embankment (4 layers)] and less lateral movement soil. The strain increased with base accelerations. Increasing the base accelerations creates shaking of the soil embankment and amplification was also increased (Higher lateral movement). The strain analysis resembles the results presented by Wang et al. (2015). Results from By PLAXIS 3D analysis showed that strain (%) [Profile for tests ST1(P), ST9(P), ST19(P), and ST27(P)] also at all elevations strain (%) variation was directly proportional, according to Figure 20. The figure also shows that the maximum strain (%) was 3.60 at an acceleration of 0.20g, but dropped to 3.06 at an acceleration of 0.05 g. The highest and lowest Strain (%) from PLAXIS 3D was 4.35% and 7.37% more than the shake table model test respectively. Furthermore, Figure 23 shows the strain contour from PLAXIS 3D output results at the end program of strain response.

Table 8 Response of Strain (Experimental and numerical)

Test Name	Parameters	Layer of sand layer/ Location	Experimental Results (%)	Numerical results (%)	Variation of Results (%)
ST1	Acceleration	Sg1 (Bottom)	2.00	2.14	7.00
		Sg4 (Top)	2.85	3.06	7.37
ST9		Sg1 (Bottom)	2.20	2.37	7.73
		Sg4 (Top)	3.10	3.44	10.97
ST19		Sg1 (Bottom)	2.35	2.49	5.96
		Sg4 (Top)	3.30	3.58	8.48
ST27		Sg1 (Bottom)	2.41	2.56	6.22
		Sg4 (Top)	3.45	3.60	4.35
ST1	Surcharge	Sg1 (Bottom)	2.00	2.14	7.00
		Sg4 (Top)	2.85	3.06	7.37
ST35		Sg1 (Bottom)	2.80	3.16	12.86
		Sg4 (Top)	3.30	3.52	6.67
ST67		Sg1 (Bottom)	3.10	3.24	4.52
		Sg4 (Top)	3.55	3.81	7.32
ST1	Frequency	Sg1 (Bottom)	2.00	2.14	7.00
		Sg4 (Top)	2.85	3.06	7.37
ST2		Sg1 (Bottom)	1.80	2.06	14.44
		Sg4 (Top)	2.71	2.86	5.54
ST3		Sg1 (Bottom)	1.40	1.56	11.43
		Sg4 (Top)	2.68	2.83	5.60
ST4		Sg1 (Bottom)	0.90	0.98	8.89
		Sg4(Top)	2.35	2.64	12.34

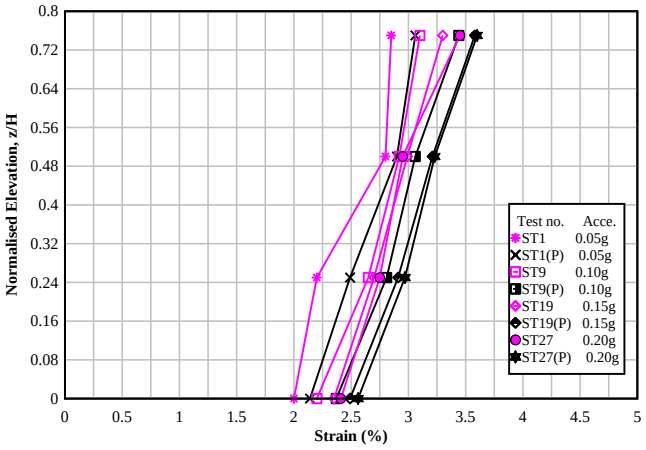

Figure 20 Effect of base acceleration on strain (ST1, 9, 19, and 27)

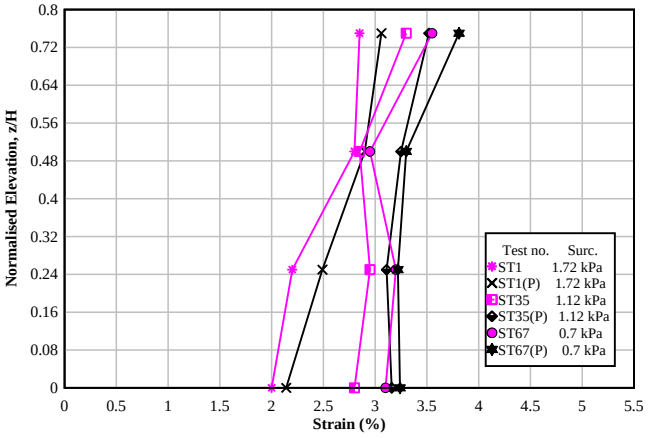

Figure 21 Effect of surcharge on strain (ST1, 35, and 67)

6.2.2 Effect of Surcharge

The strain (%) profile for tests ST1, ST35, and ST67 tested at 0.05g base acceleration and 1 Hz frequency delivered perception about the results of different surcharge loadings of 1.72 kPa, 1.12 kPa, and 0.7 kPa (Figure 21). The strain (%) values were contrariwise proportional to the surcharge pressure at all elevations. For a surcharge pressure of 0.7 kPa, the maximum strain (%) of the wall was 3.55, but the maximum strain dropped to 2.00 when the surcharge pressure was 1.72 kPa. Also, the maximum strain (%) was 3.55 for a surcharge pressure of 0.7 kPa but dropped to 2.00 for a surcharge pressure of 1.72 kPa. Strain at the peak height was contrariwise proportional to the surcharge pressure. Increasing the surcharge pressure, overburden pressure will be increased. So, the soil will be less deformed due to less lateral movement. PLAXIS 3D analysis also showed that strain (%) [Profile for tests ST1(P), ST35(P), and ST67(P)] varied was inversely proportionally with Surcharge Pressure. The maximum strain (%) was 3.81 for a surcharge pressure of 0.7 kPa, which dropped to 2.14 at a surcharge of 1.72 kPa. The highest and lowest Strain (%) from PLAXIS 3D was 7.32% and 7.37% more than the results found from the shake table test.

6.2.3 Effect of Input Frequency

Figure 22 shows that the strain (%) varies inverse proportionally with frequency. The standardized strain (%) profile was experienced for ST1, ST2, ST3, and ST4. The corresponding frequencies were 1 Hz, 2 Hz, 3 Hz, and 5 Hz, respectively, tested at 0.05g base acceleration and 1.72 kPa surcharge pressure (Figure 22). The strain (%) that occurred at z/H = 0.75 was higher than the earlier demonstrated test range. The maximum strain (%) of 2.85 was for 1 Hz frequency at z/H = 0.75. The figure also illustrated that the maximum strain (%) was 2.85 at a frequency of 1 Hz, then decreased to 2.35 at a frequency of 5 Hz. The PLAXIS 3D analysis also showed that at all elevation

strain values (%) [Profile for tests ST1(P), ST2(P), ST3(P), ST4(P), ST5(P), ST6(P), ST7(P), and ST8(P)] were inversely proportional with frequency. It also shows that the maximum strain (%) was 3.06 at a frequency of 1 Hz, which later was reduced to 2.64 at a frequency of 5 Hz. The highest and lowest strain (%) from PLAXIS 3D were 12.34 and 7.37, respectively, signifying the values are more than the shake table test.

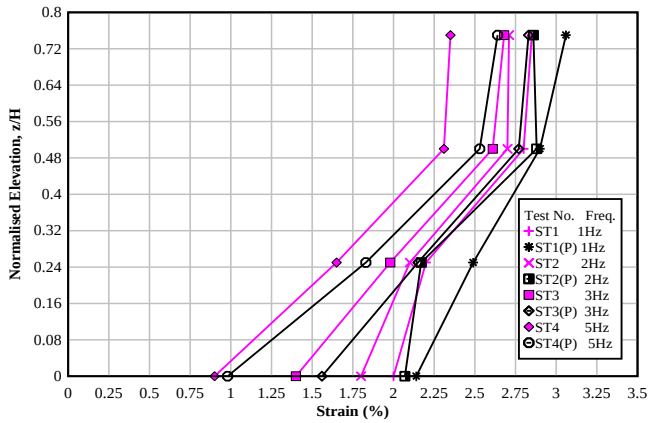

Figure 22 Effect of frequency on strain (ST1-ST4)

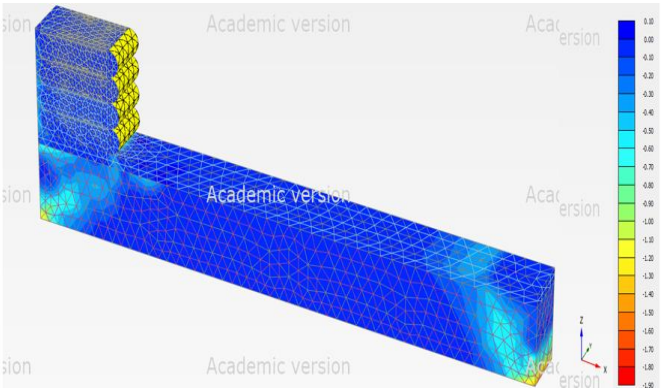

Figure 23 Strain Contour at the end (ST1)

7. CONCLUSIONS

From the results and discussion sections described above, Acceleration response, Displacement, Pore Water Pressure, and Strain were measured in perspective with two parameters, Input base acceleration, frequency (1 Hz to 5 Hz), and Surcharge pressure. The tests were done both Experimentally in Shake Table and numerically with PLAXIS 3D. The input base acceleration was measured for 0.05g, 0.10g, 0.15g, and 0.20g; and the Surcharge load effects were measured for 1.72 kPa, 1.12 kPa, and 0.7 kPa for all experiments with a fixed relative density of 48%. Various dynamic soil parameters like acceleration amplification, displacement, pore water pressure, and strain for embankment were summarized below:

1) The pore water pressure response against base acceleration variation was directly proportional to both experimental and numerical analysis. The pore water pressure response against surcharge variation was inversely proportional at all elevations. On the other hand, the pore water pressure against frequency variation was directly proportional.
2) Strain (%) was relatively high at higher base accelerations at the highest elevation. The strain (%) response against surcharge variation was inversely proportional at all elevations. On the other hand, the strain (%) response against frequency variation was directly proportional.
3) The Numerical Analysis results were almost similar to the experimental study done by Shake Table Tests showing a slightly higher value confined within 15% more to the experimental results.

These findings from this study will help us to predict the dynamic behavior better and with these results, we can adjust the design parameter at our discretion. This study will provide us with a better understanding of the design and will help us to understand the effect of earthquake input in a structure.

8. REFERENCES

Anastasopoulos, I., Georgarakos, T., Georgiannou, V., Drosos, V., and Kourkoulis, R. (2010) "Seismic performance of bar-mat reinforced-soil retaining wall: Shaking table testing versus numerical analysis with modified kinematic hardening constitutive model." Soil Dynamics and Earthquake Engineering, Vol. 30, No. 10, pp1089-1105.

Bathurst, R.J., and Hatami, K. (1998) “Seismic response analysis of a geosynthetic reinforced soil retaining wall.” Geosynthetics International 5 (1–2), pp127–166.

Bhattacharjee, A., and Krishna, A. M. (2013) "Strain Behavior of Backfill Soil of Wrap Faced Reinforced Soil Walls: A Numerical Study." In Proceedings of the 18th Southeast Asian Geotechnical Conference, Advances in Geotechnical Infrastructure, pp1-6.

Brinkgreve, R.B.J., and Broere, W. (2006) Plaxis 3D foundation version 1.5. Plaxis B.V., Delft, Netherlands.

Chen, G., Zuo, X., Zhuang, H., and DU, X. (2008) "A comparison between large-size shaking table test results and numerical simulation of a subway station structure." Earthquake Engineering and Engineering Vibration-Chinese Edition, Vol. 28, No. 1, pp157.

Chen, J., Shi, X., and Li, J. (2010) "Shaking table test of utility tunnel undernon-uniform earthquake wave excitation." Soil Dynamics and Earthquake Engineering, Vol. 30, No. 11, pp1400–1416.

Cheng, X., Cui, C., Sun, Z., Xia, J., and Wang, G. (2018) “Shaking Table Test and Numerical Verification for Free Ground Seismic Response of Saturated Soft Soil.” Mathematical Problems in Engineering, 2018, pp1–14. doi:10.1155/2018/3416315

Chakraborty, S., Hore, R. Ahmed, F., and Ansary, M. A. (2017) “Soft ground improvement at the Rampal Coal Based Power Plant Connecting Road Project in Bangladesh,” Geotechnical Engineering Journal of the SEAGS & AGSSEA.

Chakraborty, S., Hore, R., Shuvon, A.M. and Ansary, M.A. (2021) “Dynamic Responses of Reinforced Soil Model Wall on Soft Clay Foundation,” Geotechnical and Geological Engineering. https://doi.org/10.1007/s10706-020-01665-z

Chakraborty, S., Hore, R., Shuvon, A. M., and Ansary, M. A. (2021) “Physical and numerical analysis of reinforced soil wall on clayey foundation under repetitive loading: effect of fineness modulus of backfill material,” Arabian Journal of Geosciences, 14(12):1-20. DOI:10.1007/s12517-021-07317-7

Damians, I.P., Bathurst, R.J., and Olivella, S. (2021) “3D modeling of strip reinforced MSE walls,” Acta Geotechnica, 16, pp711–730 https://doi.org/10.1007/s11440-020-01057-w

Edinçliler, A., and Güler, E. (1999) "Geotextile-reinforced embankments on soft clays - effects of a foundation soil crust strengthened by lime diffusion," Geosynthetics International, Vol. 6, No. 2, pp71–91.

Elgamal, A., Parra, E., Yang, Z., and Adalier, K. (2002) "Numerical analysis of embankment foundation liquefaction countermeasures," Journal of Earthquake Engineering, Vol. 6, No. 4, pp447-471.

El-Emam, M. M., and Bathurst, R. J. (2007) "Influence of reinforcement parameters on the seismic response of reduced-scale reinforced soil retaining walls," Geotextiles and Geomembranes, Vol. 25, No. 1, pp33–49.

Edinçliler, A., and Toksoy, Y. S. (2017) "Shake Table Tests to Measure the Dynamic Performance of Geotextile-reinforced Embankment," Periodica Polytechnica Civil Engineering, Vol. 61, No. 4, pp803-814.

El-Emam, M. M. (2018) "Experimental verification of current seismic analysis methods of reinforced soil walls," Soil Dynamics and Earthquake Engineering, Vol. 113, pp241-255.

Gidday, B. G., and Mittal, S. (2020) "Improving the characteristics of dispersive subgrade soils using lime," Heliyon, 6(2), e03384. DOI: 10.1016/j.heliyon. 2020.e03384

Huang, C. C., and Wang, W. C. (2005) "Seismic displacement of a geosynthetic-reinforced wall in the 1995 Hyogo-Ken Nambu earthquake," Soils and Foundations, Vol. 45, No. 5, pp1-10.

Helwany, S., Wu, J. T., Meinholz, P., Alizadeh, V., and Ghaderi, R. (2017) "Seismic behavior of GRS bridge abutments with concrete block facing: an experimental study" Transportation Infrastructure Geotechnology, 4(4), pp85-105.

Hore, R., M. R. Arefin, and Ansary, M. A. (2019) "Development of Zonation Map Based on Soft Clay for Bangladesh," Journal of Engineering Science 10(1), 2019, pp13-18.

Hore, R., Chakraborty, S., and Ansary, M. A. (2019) "Field Investigation to Improve Soft Soils Using Prefabricated Vertical Drain," Transportation Infrastructure Geotechnology. https://doi.org/10.1007/s40515-019-00093-8.

Hore, R., Chakraborty, S., Shuvon, A. M., and Ansary, M. A. (2020) "Effect of Acceleration on Wrap Faced Reinforced Soil Retaining Wall on Soft Clay by Performing Shaking Table Test", Proceedings of Engineering and Technology Innovation.

Hore, R., Chakraborty, S., Bari, M. F., Shuvon, A. M., and Ansary, M. A. (2020) "Soil Zonation and The Shaking Table Test of The Embankment on Clayey Soil," Geosfera Indonesia. https://doi.org/10.19184/geosi.v5i2.17873)

Hore, R., Chakraborty, S., and Ansary, M. A. (2020) "Experimental Investigation of Embankment on Soft Soil Under Cyclic Loading: Effect of Input Surcharges," Journal of Earth Engineering (JEE) Vol. 5, No. 1.

Hore, R., Chakraborty, S. and Ansary, M.A. (2021) "Seismic Response of Embankment on Soft Clay Based on Shaking Table Test," International Journal of Geosynthetics and Ground Engineering," 7, 3. https://sci-hub.se/https://doi.org/10.1007/s40891-020-00246-7.

Hore, R., Chakraborty, S., Shuvon, A. M., and Ansary, M. A. (2021) "Dynamic Response of Reinforced Soil Retaining Wall Resting on Soft Clay," Transportation Infrastructure Geotechnology. https://doi.org/10.1007/s40515-021-00156-9

Hore, R., Chakraborty, S. and Ansary, M.A. (2022) "Investigation of model retaining wall on soft soil," Web of Scientist: International Scientific Research Journal, Volume 3, Issue 2. DOI: 10.17605/OSF.IO/QKPVS.

Jafarzadeh, F., Faghihi, D., and Ehsani, M. (2008) "Numerical Simulation of Shaking Table Tests on Dynamic Response of Dry Sand," In 14th World Conference on Earthquake Engineering, pp1-8.

Kokusho, T. (1980) "Cyclic triaxial test of dynamic soil properties for wide strain range," Soils and foundations 20, pp45–60.

Kramer, S. L. (1996) "Geotechnical Earthquake Engineering," Prentice Hall, Upper Saddle River, NJ, 653.

Krishna, A. M., and Latha, G.M. (2007) "Seismic response of wrap-faced reinforced soil retaining wall models using shaking table tests," Geosynthetics International, Vol. 14, No. 6, pp355-364.

Kanty, P., Sternik, K., and Kwiecień, S. (2016) "Numerical analysis of consolidation of embankment subsoil reinforced with dynamic replacement stone columns," Czasopismo Techniczne, pp79-100.

Latha, G. M., and Krishna, A.M. (2006) "Shaking Table Studies on Reinforced Soil Retaining Walls," Indian Geotechnical Journal, Vol. 36, No. 4, pp321-333.

Ling, H. I., Mohri, Y., Leshchinsky, D., Christopher B., Matsushima, K., and Liu, H. (2005) "Large-scale shaking table tests on modular-block reinforced soil retaining walls," Journal of Geotechnical and Geoenvironmental Engineering, ASCE, Vol. 131, No. 4, pp465–476.

Latha, G. M., and Manju, G. S. (2016) "Seismic Response of Geocell Retaining Walls Through Shaking Table Tests," International Journal of Geosynthetics and Ground Engineering, 2(1), 7.

Li, J., Xiang, N., Tang, H., and Guan, Z. (2016) "Shake-table tests and numerical simulation of an innovative isolation system for highway bridges," Soil dynamics and earthquake engineering, Vol. 86, pp55-70.

Matsuo, O., Tsutsumi, T., Yokoyama, K., and Saito, Y., (1998) "Shaking table tests and analysis of geosynthetic-reinforced soil retaining walls," Geosynthetics International 5 (1–2), pp97–126.

Moss, R. E., Crosariol, V., and Kuo, S. (2010) "Shake Table Testing to Quantify Seismic Soil-Structure Interaction of Underground Structures," Proc., Int. Conf. on Recent Advances in Geotechnical Earthquake Engineering and Soil Dynamics, Univ. of Missouri, Rolla, MO.

Richardson, G. N., and Lee, K. L. (1975) "Seismic design of reinforced earth walls," Journal of the Geotechnical Engineering Division, ASCE, Vol. 101, No. 2, pp167–188.

Sakaguchi, M., Muramatsu, M., and Nagura, K. (1992) "A discussion on reinforced embankment structures having high earthquake resistance," Proceedings of the International Symposium on Earth Reinforcement Practice, IS-Kyushu 92, Fukuoka, Japan, Vol. 1, pp287–292.

Sakaguchi, M. (1996) "A study of the seismic behavior of geosynthetic reinforced walls in Japan," Geosynthetics International, Vol. 3, No. 1, pp13–30.

Sabermahani, M., Ghalandarzadeh, A., and Fakher, A. (2009) "Experimental study on seismic deformation modes of reinforced-soil walls," Geotextiles and Geomembranes, Vol. 27, No. 2, pp121-136.

Srilatha, N., Latha, G. M., and Puttappa, C. G. (2013) "Effect of frequency on seismic response of reinforced soil slopes in shaking table tests," Geotextiles and Geomembranes, Vol. 36, pp27–32.

Srilatha, N., Madhavi Latha, G., and Puttappa, C.G. (2014) "Shaking Table Studies on Geotextile Reinforced Soil Slopes," Golden Jubilee Conference of the IGS Bangalore Chapter, Geo-Innovations, 30-31 October 2014, pp1-8

Wu, Y., Lu, J., and Qi, A. (2019) "Shaking table test and numerical analysis of mid-story isolation eccentric structure with tower–podium," Advances in Mechanical Engineering, Vol. 11, No. 1, pp1-16. DOI: 10.1177/1687814018819562

Wulandari, P. S., and Tjandra, D. (2015) "Analysis of geotextile reinforced road embankment using PLAXIS 2D," The 5th International Conference of Euro Asia Civil Engineering Forum (EACEF-5), Procedia Engineering, 125, pp358 – 362.

Yu, P., and Richart, F.E. (1984) "Stress ratio effects on shear modulus of dry sands," Journal of Geotechnical Engineering, ASCE 110 (GT3), pp331–345.

Yegian, M. K., Kadakal, U., and Catan, M. (1999) "Geosynthetics for earthquake hazard mitigation," In: Geosynthetics '99: Specifying Geosynthetics and Developing Design Details. Vol. 1, pp87–100.

Yazdandoust, M. (2017) "Investigation on the seismic performance of steel-strip reinforced-soil retaining walls using shaking table test," Soil Dynamics and Earthquake Engineering, 97, Elsevier, pp216-232.

Zhang, Z., Cho, C., Pan, Q., and Lu, X. (2009) "Experimental Investigation on Excess Pore Water Pressure in Soft Soil-Foundations under Minor Shocks," International Journal of Engineering and Applied Sciences, 5(4), pp259-263.

Zhou, Z., Lei, J., Shi, S., and Liu, T. (2019a) "Seismic Response of Aeolian Sand High Embankment Slopes in Shaking Table Tests." Applied Sciences, Vol. 9, pp1677.

Zhou, Y., Chen, P., Zhang, L., Wang, C., and Lu, Z. (2019b) "Shaking table tests and numerical analysis of an over-track multi-tower building," Structure and Infrastructure Engineering, Vol. 15, No. 2, pp230-243.